A Tomato Tocopherol Binding Protein Sheds Light on Intracellular -tocopherol Metabolism in Plants

Bermúdez, Luisa; del Pozo, Talía; Lira, Bruno Silvestre; de Godoy, Fabiana; Boos, Irene; Romanó, Cecilia; Previtali, Viola; Almeida, Juliana; Bréhélin, Claire; Asis, Ramón

Published in:
Plant and Cell Physiology

Link to article, DOI:
10.1093/pcp/pcy191

Publication date:
2018

Document Version
Peer reviewed version

Title: A Tomato Tocopherol Binding Protein Sheds Light on Intracellular α-tocopherol Metabolism in Plants

Running head: SlTBP affects tocopherol metabolism

Corresponding Authors Information:

Name: Magdalena Rossi
Address: Departamento de Botânica, Instituto de Biociências, Universidade de São Paulo, Rua do Matão, 277, 05508-900, São Paulo, Brasil.
Phone: 55-11-3091-8063
E-mail: mmrossi@usp.br

Name: Fernando Carrari
Address: Instituto de Biotecnología, CICVYA-INTA, P.O. BOX 25, B1712WAA Castelar, Argentina.
Phone: 54-11-4621-1447.
E-mail: carrari.fernando@inta.gob.ar

Subject area: Proteins, enzymes and metabolism

Total Figures: 5
Colour Figures: Fig. 1, 2, 3 and 5.
Black and White Figures: Fig. 4
Tables: 2
Supplementary Figures: 7
Supplementary Tables: 9

Title: A Tomato Tocopherol Binding Protein Sheds Light on Intracellular α-tocopherol Metabolism in Plants

Running head: SlTBP affects tocopherol metabolism

Luisa Bermúdez[1], Talía del Pozo[2], Bruno Silvestre Lira[3], Fabiana de Godoy[3], Irene Boos[4], Cecilia Romanó[4], Viola Previtali[4], Juliana Almeida[3†], Claire Bréhélin[5], Ramón Asis[6], Leandro Quadrana[1,¥], Diego Demarco[3], Saleh Alseekh[7], Rigel Salinas Gamboa[8], Laura Pérez-Flores[8], Pia Guadalupe Dominguez[1,‡], Christophe Rothan[9], Alisdair Robert Fernie[7], Maurício González[10], Achim Stocker[11], Andrea Hemmerle[11], Mads Hartving Clausen[4], Fernando Carrari[1,3,§,*] and Magdalena Rossi[3,§,*]

1 Instituto de Biotecnología, Instituto Nacional de Tecnología Agropecuaria (IB-INTA), and Consejo Nacional de Investigaciones Científicas y Técnicas (CONICET), PO Box 25, B1686WAA Castelar, Argentina.
2 Centro de Conservación y Propagación Vegetal (CEPROVEG), Facultad de Ciencias, Universidad Mayor, Santiago, Chile.
3 Departamento de Botânica, Instituto de Biociências, Universidade de São Paulo, Rua do Matão, 277, 05508-090, São Paulo, Brazil.
4 Center for Nanomedicine and Theranostics, Department of Chemistry, Technical University of Denmark, Kemitorvet 207, 2800, Kgs. Lyngby, Denmark.
5 CNRS, Laboratory of Membrane Biogenesis, UMR 5200, 33140 Villenave d´Ornon Cedex, France.
6 CIBICI, Facultad de Ciencias Químicas, Universidad Nacional de Córdoba, CC 5000, Córdoba, Argentina.
7 Max Planck Institute of Molecular Plant Physiology, Wissenschaftspark Golm, Am Mühlenberg 1, Potsdam-Golm, D-14476, Germany.
8 Laboratorio de Fisiología, Bioquímica y Biología Molecular de Plantas, Departamento de Ciencias de la Salud DCBS, Universidad Autónoma Metropolitana, 09340 Iztapalapa, Mexico, D.F., Mexico.
9 INRA-Bordeaux. Fruit Biology and Pathology Unit. F-33883 Villenave d'Ornon. France.
10 Laboratório de Genética Molecular Vegetal, Universidad de Chile. Macul 13 5540, Santiago de Chile, Chile.
11 Department of Chemistry and Biochemistry, University of Berne, Freiestrasse 3, 3012 Berne, Switzerland.

§These authors contributed equally to this work.

† Present address: School of Biological Sciences, Royal Holloway University of London, Egham, Surrey, TW20 0EX, UK.
¥ Present address: Institut de Biologie de l'Ecole Normale Supérieure, Centre National de la Recherche Scientifique, Institut National de la Santé et de la Recherche Médicale, Ecole Normale Supérieure, Paris, France.

‡ Present address: Department of Forest Genetics and Plant Physiology, Umea Plant Science Center. Sweden

*Corresponding Authors Contact:

Name: Magdalena Rossi

E-mail: mmrossi@usp.br

Name: Fernando Carrari

E-mail: carrari.fernando@inta.gob.ar

ABSTRACT

Tocopherols are non-polar compounds synthesized in the plastids, which function as major antioxidants of the plant cells and are essential in the human diet. Both the intermediates and final products of the tocopherol biosynthetic pathway must cross plastid membranes to reach their sites of action. So far, no protein with tocopherol binding activity has been reported in plants. Here, we demonstrated that the tomato SlTBP protein is targeted to chloroplasts and able to bind α-tocopherol. *SlTBP*-knockdown tomato plants exhibited reduced levels of tocopherol in both, leaves and fruits. Several tocopherol-deficiency phenotypes were apparent in the transgenic lines, such as alterations in photosynthetic parameters, dramatic distortion of thylakoid membranes and significant variations in the lipid profile. These results, along with the altered expression of genes related to photosynthesis, tetrapyrrole, lipid, isoprenoid, inositol/phosphoinositide and redox metabolisms suggest that SlTBP may act conducting tocopherol (or its biosynthetic intermediates) between the plastid compartments and/or at the interface between chloroplast-ER membranes, affecting inter-organellar lipid metabolism.

KEYWORDS: lipid metabolism, organelle communication, *Solanum lycopersicum*, tocopherol metabolism, tomato.

INTRODUCTION

Tocopherols are non-polar compounds synthesized in the plastids of photosynthetic organisms. They are important lipid soluble antioxidants that function as major photosynthetic activity protectants by scavenging singlet oxygen ($^1O_2$) and lessening the extent of lipid peroxidation (Miret and Munné-Bosch, 2015). Together with tocotrienols, tocopherols constitute the vitamin E (VTE) group of compounds, which are distinguished by the degree of saturation of their prenyl moiety and the methylation pattern of their polar head. These compounds are synthesized *de novo* from a hydrophilic chromanol group and a prenyl side chain produced by the shikimate and methylerythritol phosphate (MEP) pathways, respectively (Miret and Munné-Bosch, 2015). For tocopherols, phytyl diphosphate (PDP) side chain prenylation by homogentisate phytyltransferase (VTE2) converts homogentisate (HGA) into 2-methyl-6-phytyl-1,4- benzoquinone (MPBQ). Tocopherol cyclase (VTE1) catalyzes chromanol ring synthesis leading to the formation of δ-tocopherol. Alternatively, MPBQ methylation, by MPBQ methyltransferase (VTE3), results in 2,3-dimethyl-6-phytyl-1,4-benzoquinone (DMPBQ), whose cyclization by VTE1 leads to the formation of γ-tocopherol. The addition of a methyl group to the sixth position of the chromanol ring, by γ-tocopherol methyltransferase (VTE4) converts δ-tocopherol and γ-tocopherol into β-tocopherol and α-tocopherol, respectively. In addition to the pathway of the *de novo* synthesis, the PDP precursor may also originate from the recycling of the phytol moiety released from chlorophyll turnover or degradation, by the action of phytol kinase (VTE5) (Valentin, 2006) and phytyl phosphate kinase (VTE6) (vom Dorp *et al.*, 2015). Tocotrienols are synthesized from the condensation of HGA with geranylgeranyl diphosphate (GGDP) by the action of a specific transferase (HGGT, homogentisate geranylgeranyltransferase). The resultant 2-methyl-6-geranylgeranyl benzoquinol (MGGBQ) is modified, in a similar manner to tocopherols, by VTE1, VTE3 and VTE4 to further produce α-, β-, δ- and γ-tocotrienols.

Although most of the enzyme activities involved in the biosynthesis of tocochromanols have been localized at the inner membrane of the chloroplast envelope (Spicher and Kessler, 2015), the key step of cyclization is carried out by VTE1 in plastoglobules (PG) (Vidi *et al.*, 2006). Moreover, HGA biosynthesis occurs in the cytosol (Wang *et al.*, 2016). These facts implicates that biosynthetic intermediates must traffic between the inner membrane and the PG (Spicher and Kessler, 2015) and between the cytoplasm and plastids (Pellaud and Mène Saffrané, 2017).

The study of tocopherol deficient plants has provided evidence concerning the exchange of chemically diverse metabolites between the plastid and extraplastidic environments. *Arabidopsis thaliana vte2* mutants showed altered composition of lipids, mostly of those generated *via* the endoplasmic reticulum (ER) pathway (Maeda *et al.*, 2008). Similar changes in ER fatty acid profile were observed in tomato VTE5 deficient plants grown both under normal (Almeida *et al.*, 2016) and high light and temperature conditions (Spicher *et al.*, 2017). Genetic evidences suggest that these alterations in extra-plastidic lipid metabolism in VTE deficient plants are mediated by ER fatty acid desaturases (Maeda *et al.*, 2008; Song *et al.*, 2010). This means that plastid-synthetized tocopherol, and/or its related metabolites, should be accessible for the ER, directly or indirectly influencing ER-resident enzymes. Two different, yet non-mutually exclusive models have been proposed to explain

transorganellar communication: an intermembrane transporter-based model and a model based on membrane hemi-fusion between organellar membranes (Mehrshahi *et al.*, 2014). These models could also be applicable to the intraorganellar traffic of tocopherol biosynthetic intermediates between the inner membrane and PG described above. Although the membrane hemi-fusion model is supported by transorganellar complementation of *vte1* Arabidopsis mutant plants (Mehrshahi *et al.*, 2013), neither proteins with tocopherol-related compound binding activity, nor contact between the PG and envelope have been described in plants (Austin, 2006). This constitutes a current research gaps on intraplastidial and chloroplast-ER communication.

Previous studies using a *Solanum pennellii* introgression line population identified a major quantitative trait loci (QTL) for tomato fruit tocopherol content on chromosome 9 (Almeida *et al.*, 2011; Schauer *et al.*, 2006). This QTL co-localised with a *locus* encoding a SEC14-like protein (Almeida *et al.*, 2011). Some members of this protein family have shown to be involved in tocopherol transport in mammalian cells and in lipid traffic in yeasts and plants (Saito *et al.*, 2007; Bankaitis *et al.*, 2010). In this work, we show that this protein, hereafter named SlTBP (*Solanum lycoperisicum* tocopherol binding protein), is a homolog of the human α-tocopherol transfer protein (HsTTP) (Meier *et al.*, 2003), which has intermembrane α-tocopherol transfer activity mediated by phosphatidylinositol phosphates (PIPs) (Kono *et al.*, 2013). By functional characterization of SlTBP, we provide insights about this plastidial protein involved in intracellular traffic of α-tocopherol in plants.

RESULTS

SlTBP encodes a chloroplast targeted protein of the patellin family and is highly expressed in green tissues

In order to evaluate the diversity of SEC14-like proteins in plants, the Phytozome v10.2 database was surveyed using SlTBP as bait (Solyc09g015080). This sequence was found to belong to the cluster id 55282292, a gene family that comprises 286 members annotated as "Hypothetical Viridiplantae genes" associated to lipid transport and metabolism. Of these genes, 147 sequences encompassing 24 Angiosperm species were selected to perform a phylogenetic analysis. Additionally, the functionally characterized SEC14 protein from *Saccharomyces cerevisiae* (Tanksley, 2004), ScSEC14, and the *Homo sapiens* proteins TOCOPHEROL TRANSFER PROTEIN, HsTTP (Nava *et al.*, 2006), and SUPERNATANT PROTEIN FACTOR, HsSPF (Stocker and Baumann, 2003), were included in the analysis and used as queries for retrieving *Mus musculus, Drosophila melanogaster, Homo sapiens* and *Bombyx mori* homologs (Supplementary Table S1).

The phylogenetic reconstruction revealed three clearly defined plant clades, which were named according to their *Arabidopsis thaliana* homologs (Peterman, 2004; Peterman *et al.*, 2006). ScSEC14 remained as an out group, while the Animalia sequences were divided into two clades, HsTTP-like and HsSPF-like, indicating an ancestral duplication within this kingdom. The clades containing AtPATL4-like and AtPATL6, with the later including SlTBP, split before the divergence of Eudicots and Monocots. Yet a duplication following the divergence of the basal order Ranunculales, which includes *Aquilegia coerulea*, increased diversity in Eudicots species originating two distinct clades, AtPATL1/2 and AtPATL3/5 (Figure 1a).

The proteins from the plant and the Hs-SPF-like clades exhibit three known and conserved domains in all sequences: (i) a CRAL-TRIO domain (IPR001251, CELLULAR RETINALDEHYDE BINDING PROTEIN and the TRIO guanine exchange factor), which binds small lipophilic molecules such as retinaldehyde and α-tocopherol (Panagabko *et al.*, 2003), (ii) the CRAL-TRIO N-terminal (IPR011074), an alpha-helix rich region with unknown function found at the N-terminal region of CRAL-TRIO domains; and (iii) the GOLD domain (IPR009038, GOLGI DYNAMICS) that is predicted to mediate interaction with other proteins (Anantharaman and Aravind, 2002) (Figure 1a).

In order to gain information concerning the subcellular localization of SEC14 proteins, the presence of putative plastidial signal peptides was *in silico* investigated. Of the 147 plant sequences, 22 were predicted to be plastid-targeted (Supplementary Table S1). Interestingly, 19 of them are members of the AtPATL6 SlTBP clade (Figure 1b), suggesting that this group is characterized by the presence of a chloroplast signal peptide. The prediction of SlTBP as a plastidial protein was confirmed by the transient expression of a GFP (*green fluorescence protein*) fusion protein in *Nicotiana benthamiana* leaves, where the confocal visualization of the fluorescence revealed that SlTBP is targeted to the chloroplasts (Figure 1c). Regarding the expression of *SlTBP*, the mRNA corresponding to this gene was detected both in leaves and fruits, however its expression levels were considerably higher in green tissues, being 250-fold more expressed in sink leaves than in ripe fruits (Figure 1d).

SlTBP binds to α-tocopherol

Given that the *SlTBP* gene was identified to be associated to a tocopherol QTL (Schauer *et al.*, 2005; Almeida *et al.*, 2011) and due to its homology to HsTTP (Min *et al.*, 2003), we next explored its α-tocopherol binding activity. First, we compared the predicted amino acid sequence and the 3D structure of tomato and human polypeptides. Despite exhibiting a modest overall identity of 24.8%, structural alignment revealed that both proteins are highly similar including the α-tocopherol binding pocket (Min *et al.*, 2003) (Supplementary Figure S1). Interestingly, out of the 13 residues that interact with the ligand, two are identical and seven are similar (Supplementary Figure S1b), supporting the hypothesis of conserved function.

Based on this observation, the His-tagged tomato protein was expressed in *Escherichia coli* (BL21AI) and the production of a recombinant protein was confirmed by Western blot analysis with anti-His antibody (Figure 2a). SlTBP-α-tocopherol binding was tested by affinity chromatography using an α-tocopherol-biotin conjugate immobilized on a streptavidin column. After loading, the column showed retention of SlTBP protein until eluted with α-tocopherol, as shown in Figure 2b, confirming its ability to bind α-tocopherol. It is worth mentioning that column loading and elution were performed with PBS-buffer, which has no protein denaturating effect. The identity of the SlTBP eluted protein (46 KDa band) was verified by mass spectrometry sequencing (Supplementary Figure S2).

Further to improve the chromatography and evaluated the binding specificity, SlTBP was purified and binding assays repeated with tocopherol and another isoprenoid-derived lipophilic compound, phylloquinone. Results showed that SlTBP binding activity is not limited to tocopherol, raising the hypothesis of this protein might be involved in broader lipid trafficking regulation (Figure 2c).

SlTBP-knockdown plants are deficient in tocopherol and carotenoid accumulation

Having demonstrated that SlTBP binds tocopherol, the role of this protein in tomato metabolism was evaluated by the characterization of *SlTBP*-knockdown plants. Four independent RNAi lines, exhibiting a reduced expression of over 50 % in both leaves and ripe fruits, were selected for further phenotyping, hereafter referred to as L15, L18, L19 and L24 (Supplementary Figure S3). Primary metabolism was slightly affected by the silencing of *SlTBP* (Figure 3 and Supplementary Table S2). Most of the changes were observed in source leaves; 18 metabolites showed a distinct pattern of accumulation in the leaves, while only seven were affected in ripe fruits. The metabolic classes more affected by *SlTBP*-knockdown were the organic acids in leaves, specifically tricarboxylic acid cycle intermediates and those involved in ascorbate metabolism. Additionally, SlTBP deficiency led to an increase in several amino acids in both analyzed organs.

The total tocopherol content was significantly diminished in leaves and ripe fruits of the *SlTBP*-knockdown lines, by approximately 30% and 20%, respectively. By contrast, chlorophylls were unaffected by *SlTBP* silencing, however, the major carotenoids, lycopene and β-carotene, also exhibited reduced contents in ripe fruits (Table 1).

SlTBP plays a role in maintaining chloroplast structure integrity and affects lipid composition

Given that the role of tocopherol in plant growth and development is related to the stabilization of photosynthetic membranes, gas exchange and chlorophyll fluorescence parameters were measured in source leaves from 8-week-old *SlTBP*-knockdown plants (Table 2). No differences were found in transpiration rate (*E*), stomatal conductance (*gs*) or CO_2 assimilation rate (*A*). However, SlTBP deficiency resulted in reductions in electron transport rate (ETR), the proportion of open PSII centers (*qP*) and PSII operating efficiency (Φ_{PSII}), while non-photochemical quenching (NPQ) and reduced quinone acceptor (1-pQ) were increased in comparison to the wild type genotype. Although there were neither penalties on biomass accumulation nor on fruit number or weight (Supplementary Table S3), the above-mentioned results implied that SlTBP deficiency alters the energy usage of excited chlorophyll. Thus, as a parameter of oxidative stress, lipid peroxidation was estimated. Malondialdehyde (MDA) equivalent was more than doubled in the leaves of transgenic plants compared to the control genotype (Figure 4a). However, no changes in lipid peroxidation were detected in fruits (Supplementary Figure S4). Regarding the plastidial ultrastructure, *SlTBP*-knockdown led to a dramatic thylakoid grana disruption of the leaf chloroplasts (Figure 4b) and the development of smaller plastids with more and larger PG (Figure 4c).

Having demonstrated that *SlTBP* silencing affected the tocopherol levels and, consequently, impacted on photosynthetic function, lipid peroxidation and plastidial membrane ultrastructure, we next evaluated how tocopherol deficiency affects lipid metabolism. For this purpose, the lipid profile of *SlTBP*-knockdown lines was analyzed (Supplementary Table S4). In source leaves, increased levels of total neutral lipids (NL) were observed (Figure 4d), as a consequence of the increases in fatty acid phytyl esters (FAPE), triacylglycerols (TAG), free fatty acids (FFA) and diacylglycerols (DAG) (Supplementary Table S4). Interesting to note is that all the identified acyl chains (*i.e.* C16:0, C18:0, C18:1, C18:2 and C18:3) of the neutral lipids increased in the transgenic lines. Regarding fatty acid saturation level, higher linoleic acid (C18:2) total content (4.3 *vs* 6.1 μg mg DW^{-1} comparing the mean of control and transgenic lines, respectively) and a decreased C18:3/C18:2 ratio (2.0 *vs* 1.5 comparing the mean of control and transgenic lines, respectively) were observed in the leaves from *SlTBP*-knockdown lines. Except for the reduction in monogalactosyldiacyl glycerols (MGDG) (composed mainly by C18:2 and C18:3), lipid profiles from ripe fruits were almost indistinguishably between transgenic and control plants, not even alterations in fatty acid saturation levels were detected (Figure 4d).

Expression profiles of SlTBP-knockdown plants are in accordance with their phenotypic alterations

The effect of SlTBP deficiency was also assessed at the level of global gene expression. In source leaves and ripe fruits 11,474 and 11,630 genes displayed detectable expression, respectively. SlTBP deficiency resulted in up-regulation of 261 and 419 genes and down-regulation of 139 and 429 genes, respectively, in these organs (Supplementary Table S5 and Supplementary Figure S5); only 3 and 7%

of the total transcripts analysed. Subsequently, the altered expression of ~70% (50/72) of tested genes was validated by means of qPCR assay (Supplementary Table S5 and Supplementary Table S6).

The classification of the genes exhibiting altered patterns of expression revealed that *miscellaneous*, *RNA and protein metabolism*, as well as *signalling* were the functional categories most affected by SlTBP deficiency (Supplementary Figure S6). However, considering the metabolic perturbation induced by *SlTBP*-knockdown, the genes associated with photosynthesis (functional category *1 PS*), tetrapyrrole metabolism (functional category *19.99 tetrapyrrole synthesis*), lipid metabolism (functional category *11 lipid metabolism*), isoprenoid metabolism (functional category *16.1 secondary metabolism.isoprenoids*), inositol/phosphoinositides metabolism (functional categories *30.4 signalling.phosphoinositides*, *3.4 minor CHO metabolism.myo-inositol* and *34.2 tranporter.sugars-inositol*) and redox homeostasis (functional category *21 redox*) categories were manually curated and the subcellular localization of their products predicted. Figure 5 summarizes these results and shows all genes presenting altered expression in leaves (Figure 5a) and ripe fruits (Figure 5b) from the transgenic lines numbered according to Supplementary Table S5.

In source leaves, genes belonging to the photosynthesis-related categories (*1 PS, 19 tetrapyrrole synthesis* and *16.1 secondary metabolism.isoprenoids*) were mostly up-regulated in the transgenic lines. These leaves also showed alterations in the expression of redox balance-related genes, such as a *GLUTAREDOXIN* (15), *PEROXIDASES* (14) and a *PHOSPHOGLUCONOLACTONASE* (13). Lipid metabolism-related genes showing altered expression in the leaves of the transgenic belong to both prokaryotic (plastidial) and eukaryotic (ER) lipid pathways and encode a wide range of biochemical functions (6, 9, 5, 8 and 7). Finally, considering that the HsTTP transports tocopherol in a PIP-mediated manner (Kono *et al.*, 2013), the expression of the inositol/phosphoinositides-related genes was carefully inspected showing altered pattern of expression for five distinct *loci*.

A high number of genes from the selected categories showed altered expression profiles in ripe fruits from the transgenic lines. Regarding isoprenoids category, three genes directly involved in carotenoid biosynthetic pathway (61, 64 and 65) and two carotenoid catabolism-associated paralogs (66) showed altered levels of their mRNA. Moreover, four other genes (62, 63, 67 and 68) involved in metabolism of terpenoids (other than carotenoids) showed changes in their mRNA levels in the transgenics. Intriguingly, several genes associated to 13 different protein functions belonging to photosynthesis category (*1 PS)* exhibited altered expression. Additionally, a diverse set of genes (53, 56, 57, 58, 14, 52, 54 and 55) involved in redox regulation associated functions showed changes in their transcript profile; being found in different cellular compartments, such as chloroplasts, plasma membrane, ER and cytosol. The functional category exhibiting the highest number of altered genes in ripe fruits from *SlTBP*-knockdown plants was lipid metabolism, including genes involved in biosynthesis (*e.g.* acyl carriers -41 and 42- and acyl transferases -35-) and catabolism (*e.g. LIPASE* -6-, *LIPOXYGENASE* -39-), which were mostly up-regulated. These genes also belong to both prokaryotic (plastidial) and eukaryotic (ER) lipid pathways. Similarly, as described for leaves, inositol/phosphoinositides-related genes were also altered in the fruits of the transgenic lines.

DISCUSSION

In 2011, Almeida *et. al.,* identified three candidate genes within a major QTL mapped on chromosome 9 for total tocopherol content in tomato fruits. These genes were functionally characterized and demonstrated to affect this trait through different regulatory mechanisms: *SlVTE3* participates in *de novo* α-tocopherol biosynthesis (Quadrana *et al.*, 2014); *SlVTE5* regulates the availability of prenyl precursor by chlorophyll-derived phytol recycling (Almeida *et al.*, 2016) and; in this work, we present evidences concerning the functionality of *SlTBP*, which encodes a protein with a novel function in plants that affects the accumulation of VTE through its α-tocopherol binding activity.

Phylogenetic analysis presented here supports that SlTBP is a member of the SEC14 protein family, which is distributed from yeast to humans and participates in PIP-mediated lipid transport (Bankaitis *et al.*, 2010). SlTBP belongs to the plant PATELLIN gene family, whose members have been poorly characterized to date. The *A. thaliana* PATELLIN 1 and 2 (AtPATL1/2) bind phosphoinositides and participate in vesicle trafficking events (Peterman *et al.*, 2004) and membrane regeneration (Suzuki *et al.*, 2016), respectively. Given that most of the proteins of the SlTBP-containing clade are characterized by the presence of predicted chloroplast target peptides, it is more parsimonious to assume that this is an ancestral feature that was independently lost during evolution in a few members of this clade, such as the case of the *A. thaliana* ortholog (AtPATL6). Importantly, the chloroplast subcellular localization of the tomato protein was experimentally confirmed here.

A close inspection to the predicted structure of SlTBP revealed a high conservation with the CRAL-TRIO N-terminal and CRAL-TRIO domains of the human homolog HsTTP (Meier *et al.*, 2003), even with respect to the amino acid residues which interact with α-tocopherol (Min *et al.*, 2003). This observation led us to investigate whether SlTBP has tocopherol binding activity, which was confirmed by means of affinity chromatography assay with the tomato recombinant protein. However, the ability of phylloquinone to also eluate SlTBP from the tocopherol-biotin conjugate, exposed a broader spectrum of ligands for this protein that could be expanded to isoprenoid-derived lipophilic compound.

Having demonstrated that SlTBP is able to bind α-tocopherol, we further investigated the involvement of this protein in tomato plant metabolism. Analyses of RNAi-mediated *SlTBP*-knockdown lines revealed significant reductions in the total tocopherol contents (α- and γ- forms), both in source leaves and ripe fruits. This result demonstrates that SlTBP participates in the regulation of tocopherol metabolism *in vivo*. However, the impact of tocopherol deficiency on metabolite and transcript profiles in these organs was clearly different (discussed below) revealing a metabolic organ-specific adjustment, as we have previously reported for *SlVTE5*-silenced tomato plants (Almeida *et al.*, 2016). In general terms, the metabolic effect of SlTBP manipulation was more pronounced in leaves than in mature fruits; however, a higher number of genes with altered expression levels were detected in mature fruits. This is in line with the major role of transcriptional regulation over the fruit ripening process (Giovanonni *et al.*, 2017).

The role of tocopherols in protecting PSII against oxygen singlets (Krieger-Liszkay and Trebst, 2006) and in limiting lipid peroxidation (Miret and Munné-Bosch, 2015) is well documented. Consistent with

these observations, the reductions in tocopherol observed in leaves from *SlTBP*-knockdown plants coincided with significant alterations in the chlorophyll fluorescence parameters, lipid peroxidation and thylakoid membrane stacking. The changes observed in the expression of photosynthesis-related genes are in clear agreement with the observed impairments in photosynthetic light reactions, implying that the transgenic plants cannot cope with the excited chlorophyll. This hypothesis is supported by the up-regulation of the *MENAQUINONE METHYLTRANSFERASE* encoding gene (21 in Figure 5). This gene product participates in the biosynthesis of phylloquinone, which is a PSI-associated electron acceptor. Within this context it is important to note that phylloquinone and tocopherols are produced into the plastoglobuli and share biosynthetic precursors (Spicher and Kessler, 2015).

Beside the aforementioned phenotypes, the leaves of the transgenic plants exhibited increased levels of neutral lipids (i.e. FAPE, TAG, FFA and DAG), which could explain the increase in plastoglobuli number and size, where these compounds are stored (Nacir and Bréhélin, 2013). In line with these structural and biochemical changes are the alterations in the mRNA levels of a *LIPASE* (6) and a *PHOSPHOLIPASE* (7) encoding genes, enzymes involved in TAG and DAG neutral lipid metabolism (Padham *et al.*, 2007; Yang *et al.*, 2017). Furthermore, the impairment of tocopherol biosynthesis/accumulation may result in increases in free phytol – a long chain alcohol molecule - which exerts detergent-like effects resulting detrimental to membrane function (Sikkema *et al.*, 1995; Löbbecke and Cevc, 1995). By contrast, FAPE, which lack detergent-like structure, also increased in the leaves of transgenic plants, however, these are not considered toxic and in addition they are sequestered in plastoglobules (Lippold *et al.*, 2012).

In accordance with the photoinhibition phenotype displayed by the transgenic plants, cellular redox homeostasis-related genes and metabolites were significantly altered. The most obvious are the cases of dehydroascorbate, *GLUTAREDOXIN* (15) and *PEROXIDASES* (14) (Foyer and Shigeoka, 2011). An interesting example is the change in the transcript level of the *PHOSPHOGLUCONOLACTONASE* (13) gene and its corresponding product, gluconate. This enzyme of the oxidative pentose-phosphate pathway is sensitive to the redox cellular homeostasis (Hölscher *et al.*, 2014).

In ripe fruits of *SlTBP*-knockdown lines reductions in lycopene and β-carotene contents were observed. Two *CAROTENOID CLEAVAGE DIOXYGENASES* (CCDs) encoding genes, *SlCCD1* and *SlCCD4* (66), were up- and down-regulated respectively in the fruits of these plants. Plant CCDs are divided in four groups CCD1, CCD4, CCD7 and CCD8 that exhibit substrate promiscuity (Auldridge *et al.*, 2006). CCD4 activity was reported to have a negative effect on β-carotene contents in *A. thaliana* seeds (Gonzalez-Jorge *et al.*, 2013); while SlCCD1 cleaves β-carotene and lycopene (Simkin *et al.*, 2004). Thus, the altered expression of *SlCCDs* might, at least partially, explain the reduced levels of carotenoids observed in ripe fruits from transgenic plants. The up-regulation of *LYCOPENE β-CYCLASE* (65) and *PHYTOENE SYNTHASE* (64) and the down-regulation of the *LYCOPENE ε-CYCLASE* (61) encoding genes might represent a compensatory mechanism to ameliorate the reduction observed in pigment content. Additionally, the induction of *FARNESYL DIPHOSPHATE KINASE* (63) and *β-OCIMENE SYNTHASE* (62) divert the primary isopentenyl diphosphate precursor from carotenoid biosynthesis towards the production of other terpenoids, such as sitosterol and β-ocimene, respectively (Keim *et al.*, 2012; Dudareva *et al.*, 2003) . This shift in carotenogenesis

observed in the ripe fruits of the *SlTBP*-knockdown plants is suggestive of ripening delay, which means retardation in the photosynthetic machinery dismantling, explaining the altered expression of a high number of photosynthetic-associated genes. It is widely known that carotenoids and tocopherols are major components of the antioxidant machinery in response to photooxidative deleterious effect. In green tissues, a boost in the xanthophyll cycle is a compensatory mechanism to palliate tocopherol deficiency (Havaux *et al.*, 2005; Havaux *et al.*, 2007). However, even when ripening has been described as an oxidative phenomenon (Andrews *et al.*, 2004), such compensatory mechanism(s) is unknown in fruits. Our transcript profiling data showed that tocopherol and carotenoid deficiency lead to a considerable alteration in the expression of redox-associated genes as a response to maintain oxidation-reduction balance.

It has been shown that tocopherol deficiency affects extraplastidial fatty acid metabolism (Maeda *et al.*, 2008; Almeida *et al.*, 2016). The transcriptional profile of *SlTBP*-silenced plants demonstrated that alterations in lipid metabolism occurred in those genes involved in both prokaryotic and eukaryotic pathways. Knowing that the fatty acids that support galactolipid synthesis for plastidial membranes are desaturated in the ER (Li-Beisson *et al.*, 2010), the reduced levels of MGDG and the altered expression of the *MONOGALACTOSYLDIACYLGLYCEROL SYNTHASE* encoding gene (43) observed in ripe fruits likely reflect that plastid-ER interorganellar communication is altered in SlTBP-deficient plants.

Moreover, not only in fruits but also in leaves, the shift in the expression of *PHOSPHOINOSITIDE KINASES* (18) and *PHOSPHATASES* (16 and 60) encoding genes suggests that PIPs metabolism is altered in transgenic plants (Stevenson *et al.*, 2000). Reinforcing this, higher contents of inositol were detected in ripe fruits of *SlTBP*-knockdown lines. It is worth mentioning that several SEC14-like proteins have been reported to bind PIPs (KF de Campos and Schaaf, 2017; Miller *et al.*, 2015; Schaaf *et al.*, 2008). In particular, HsTTP promotes the intermembrane release of α-tocopherol in a PIP-dependent manner, and the three arginine residues (R59W, R192H and R221W) essential for PIP binding activity (Kono *et al.*, 2013) are conserved in SlTBP. The sequence conservation suggests that SlTBP could have a similar reaction mechanism as that described for the human homolog.

Evidences presented here concerning the functionality of SlTBP can be summarized as follows: (i) SlTBP is structurally similar to HsTTP, targeted to chloroplasts and binds tocopherol, (ii) *SlTBP* silencing results in a tocopherol deficiency phenotype both in leaves and in fruits, (iii) the knockdown plants display alterations in chloroplast ultrastructure and chlorophyll fluorescence parameters compatible with dysfunctional light reactions, (iv) SlTBP deficiency results in changes in lipid metabolism in both leaves and fruits and, (v) all these changes are accompanied by variations in PIP-related gene expression. Taking all these results together, two possible scenarios for the action of SlTBP can be proposed. First, SlTBP could be involved in tocopherol/PIP-mediated chloroplast-ER communication and under SlTBP deficiency, lipid metabolism is affected impacting on chloroplast ultrastructure, which in turn compromises tocopherol biosynthesis. The resulting reduction in antioxidant capacity impacts on the functionality of the photosynthetic light reaction machinery. The second possible model implies SlTBP mediates the transport of α-tocopherol (and/or its biosynthetic

intermediates/or related lipophilic molecules) between the inner envelope membrane and PG/thylakoid membranes. Thereafter, in the face of SlTBP reduction, tocopherol accumulation is compromised, PG function is altered leading to an impairment of the plastidial electron transport chain and extra-plastidial lipid metabolism is affected. The disturbed plastid ultrastructure could either be the consequence of the alteration in oxidative stress and/or the shift in lipid metabolism.

The collection of evidence as a whole, rather than any single individual data, allow to propose that SlTBP plays a novel function in plants mediating the role of tocopherol in inter/intraorganellar communication. This not only brings new insights on the intracellular traffic of nonpolar compounds, but also adds another dimension on the regulation of tocopherol metabolism which should be considered for crop nutritional improvement strategies.

EXPERIMENTAL PROCEDURES

Phylogenetic analysis

The protein sequence of all members of the SEC14 gene family in plants was obtained from the Phytozome v10.2 gene family dataset using the sequence of SlTBP as query. Sequences with less than half of the length mode (*i.e.* 213 amino acids) were removed from the analysis. Sequences of *Mus musculus, Drosophila melanogaster, Homo sapiens* and *Bombyx mori* were obtained from a BLASTp against the NCBI (https://www.ncbi.nlm.nih.gov) protein database using the functionally characterized ScSEC14, HsTTP and HsSPF as queries. Only BLAST hits with score of at least 100 were included in the analysis. Sequences were aligned by the ClustalW program in MEGA 6.0.5 software (Tamura *et al.*, 2013), which was also used for the determination of the best substitution model for phylogenetic analysis. This reconstruction was made using the Maximum Likelihood principle with PhyML 3.0 software (Guindon *et al.*, 2010) within the Phylogeny.fr server (http://phylogeny.lirmm.fr/phylo_cgi/index.cgi (Dereeper *et al.*, 2008)), the statistical test for branch support was a parametric χ^2 based test with the substitution model pointed out by the former analysis. The obtained tree was visualized and edited in MEGA 6.0.5 software.
For sequence annotation, domains were predicted by InterProScan 5 (Jones *et al.*, 2014) and ScanProsite (de Castro *et al.*, 2006), presence of a chloroplast signal peptide was evaluated using ChloroP (Emanuelsson *et al.*, 1999). The protein representation was created with Prosite MyDomains – Image Creator (http://prosite.expasy.org/mydomains/).

Expression of SlTBP in Escherichia coli

The full-length coding region of *SlTBP* was amplified with the primers indicated in Supplementary Table S9 and cloned into the pDEST17 destination vector according to the manufacturer's instructions (Gateway® Technology, Invitrogen, Carlsbad, CA, USA) using LR clonase (Invitrogen). The pDEST17-SlTBP expression clone was transferred to *E. coli* strain BL21AI by the heat shock method as described by the supplier (Invitrogen, Carlsbad, CA, USA) and the recombinant expression vectors were confirmed by PCR and digestion. Protein expression were performed as described by the supplier. Briefly, a clone was grown overnight in LB medium containing 100 mg/ml ampicillin at 37 ˚C and shaken at 180 rpm. Subsequently, cultures were diluted 1:20 in fresh LB that contained 100 mg/ml ampicillin and cultivated at 37 ˚C until the OD600 of the media reached 0.4. Recombinant fusion protein expression was then induced by the addition of 0.2% L-arabinose and cells were grown for 4 hours. Induced cultures were centrifuged at full speed after which the supernatant was aspirated and conserved as soluble fraction and frozen at -80 ˚C for subsequent Western blot or binding assays. The recombinant protein was confirmed by Western blot with anti-His antibody (GE Healthcare # 27-4710-01). As negative control an untransformed *E. coli* (BL21AI) clone was used. For the SlTBP purification, expression was performed via autoinduction in ZYM 5052 medium (1 L Medium in a 2.5L Flask) supplemented with 50µg/ml kanamycin. The medium was inoculated with 20mL overnight

culture (BL21 DE3, pET-28a Vector), incubated 4 h at 37 °C and 280 RPM, and then cooled down to 22 °C overnight. The expression was stopped approximately 18 h after inoculation (no significant change for OD600 detectable) and the cells were harvested at 6500 RPM for 30 min at 4°C. Pellets were collected and stored at -18°C until lysis and purification.

SlTBP purification

About 40g of the frozen pellet was resuspended in 400 mL lysis buffer (2xPBS, 20mM Imidazole, pH 7.5) via stirring at 4°C overnight. Resuspended cells were lysed by physical disruption with the following method: a scoop tip of DNase to the cell suspension was added, applied about 1600 bar and let the suspension flow into ambient pressure. In doing so, the rapid pressure release, led to cell lysis. This was repeated twice with the cell suspension and then 2 % (w/v) Triton X-100 was added. Lysed cell suspension was stirred for 1 h at 4 °C and then centrifuged at 9000 g for 30 min at 4 °C. The supernatant was collected and applied on a His60 Ni Superflow resin. After all suspension volume went through, the column was washed with wash buffer (2x PBS, 40 mM Imidazole, pH 7.5) until the Absorption at 280 nm stayed stable, which indicates that everything unspecific is washed from the column. In the last step, the protein was eluted from the Ni column with elution buffer (2x PBS, 300 mM Imidazole, pH 7.5), supplemented with 20 u Thrombin (digestion of the His-tag), and dialysed in 4 L 1x PBS (pH 7.5) overnight at 4 °C to get rid of the Imidazole and provide optimal reaction conditions for the thrombin cleavage.

Synthesis of biotinylated tocopherol

To synthesize (*R*)-2,5,7,8-tetramethyl-2-((4*R*,8*R*)-4,8,12-trimethyltridecyl)chroman-6-yl 5-((3a*S*,4*S*,6a*R*)-2-oxohexahydro-1*H*-thieno[3,4-d]imidazol-4-yl)pentanoate, 1.5 mL anhydrous DMF and 1.0 mL anhydrous dichloromethane were added to a solution of biotin (55.8 mg, 228 µmol) under inert atmosphere. Triethylamine (45 µL, 325 µmol) was added and the solution was cooled to 0 ˚C under stirring. Isobutyl chloroformate (45 µL, 344 µmol) was added dropwise and the mixture was stirred for 45 min at 0 ˚C. (+) α-tocopherol (21.4 mg, 49.7 µmol) and 4-(dimethylamino)-pyridine (2.0 mg, 16.4 µmol) were dissolved in 1.4 mL anhydrous dichloromethane and added to the solution. The resulting mixture was stirred at 21 ˚C for 2 days. The solution was partially concentrated in vacuum, then diluted with ethyl acetate (50 mL) and washed with water. The aqueous layer was then extracted with ethyl acetate (3 x 50 mL). The organic phase was dried over sodium sulfate, filtered, and concentrated in vacuum. The residue was purified by flash chromatography (heptane/AcOEt, 7,3 v/v) to afford the tocopherol-biotin conjugate as a colorless solid (7.7 mg, 11.7 µmol, 24%). The resulting conjugate was confirmed by MS and NMR (Supplementary Figure S7).

Affinity chromatography

Protein extract and α-tocopherol: 1 mL column volume (CV) of HiTrap™ Streptavidin HP column (GE Healthcare Bioscience AB) was flushed with 1× PBS buffer (10 CV, 1 mL/min). The tocopherol-biotin conjugate (31 mg, 47.1 µmol) was dissolved in 22 CV DMF/PBS buffer (1/10) and applied on the column (10 CV, 0.1 mL/min). Subsequently, the column was washed with PBS buffer (6 CV), which has no protein denaturating effects. Total protein extract of the BL21AI bacteria overexpressing SlTBP (0.75 mL, ~0.75 mg) was applied on the column and the breakthrough collected. The column was incubated for 10 min at 21˚C and then washed three times with 3 CV 1× PBS buffer (collected as washing step 1-3). The protein was eluted with 2 CV α-tocopherol (21 mg in 10 mL PBS, 4.9 mM), followed by a washing step (3 CV, collected as washing step 4). The fractions were analysed by SDS-Page (7.5%, Bio-Rad precast gel). 15 µL of each fraction were treated with 5 µL loading buffer (4×) and 1 µL DDT (100 mM), heated for 5 min at 95 ˚C and 10 µL was loaded on the gel. SDS-Page was stained with Coomassie blue. The identity of the eluted protein was confirmed by MALDI Mass Spectrometry peptide mapping and sequencing (MALDI-MS/MS) according to AlphalyseTM (www.alphalyse.com).

Purified SlTBP and α-tocopherol: 1 mL column volume (CV) of HiTrap™ Streptavidin HP column (GE Healthcare Bioscience AB) was flushed with 1× PBS buffer (10 CV, 1 mL/min). The tocopherol-biotin conjugate (31 mg, 47.1 µmol) was dissolved 500 µL DMF and applied on the column. Subsequently, the column was washed with PBS buffer (6 CV). Purified SlTBP (1 mL, 200 µg/mL) was applied in the column and the breakthrough collected. The column was incubated for 30 min at 21˚C and then washed five times with 5 CV 1× PBS buffer (collected as washing step 1-5). The column was then eluted with 1 mL blank (PBS with 1% Tween20). Subsequently, the protein was eluted with 2 CV α-tocopherol (21 mg in 10 mL PBS with 1% Tween20, 4.9 mM), collected as tocopherol elution, followed by a washing step (3 CV, collected as washing step 6). The fractions were analysed by SDS-Page (7.5%, Bio-Rad stain-free precast gel). 15 µL of each fraction was treated with 5 µL loading buffer (4×) and 1 µL DDT (100 mM), heated for 5 min at 80 ˚C and 10 µL was loaded on the gel. SDS-Page was visualized with Gel Doc™ EZ System.

Purified SlTBP and phylloquinone: 1 mL column volume (CV) of HiTrap™ Streptavidin HP column (GE Healthcare Bioscience AB) was flushed with 1× PBS buffer (10 CV, 1 mL/min). The tocopherol-biotin conjugate (31 mg, 47.1 µmol) was dissolved 500 µL DMF and applied on the column. Subsequently, the column was washed with PBS buffer (6 CV).

Purified Sec14 (1 mL, 200 µg/mL) was applied on the column and the breakthrough collected. The column was incubated for 30 min at 21˚C and then washed five times with 5 CV 1× PBS buffer (collected as washing step 1-5). The column was then eluted with 1 mL blank (PBS with 1% Tween20 and 1% DMF). Subsequently, the protein was eluted with 2 CV phylloquinone (22 mg in 10 mL PBS with 1% Tween20 and 1% DMF, 4.9 mM), collected as phylloquinone elutions 1 and 2, followed by a washing step (2 CV, collected as washing step 6). Then the remaining protein was eluted with α-tocopherol (21 mg in 10 mL PBS with 1% Tween20, 4.9 mM), collected as tocopherol elution. The fractions were analysed by SDS-Page (7.5%, Bio-Rad stain-free precast gel). 15 µL of each fraction was treated with 5 µL loading buffer (4×) and 1 µL DDT (100 mM), heated for 5 min at 80 ˚C and 10 µL was loaded on the gel. SDS-Page was visualized with Gel Doc™ EZ System.

Plant material

Tomato, *Solanum lycopersicum* L. (cv Moneymaker), and *Nicotiana benthamiana* seeds were obtained from Meyer Beck (Berlin). *S. lycopersicum* (inbred variety M82, Acc LA3475) used for *SlTBP* expression analysis was kindly provided by CM Rick, Tomato Genetics Resource Center (TGRC). Plants were grown under greenhouse conditions: 16/8 h photoperiod, 24 ± 3°C, 60% humidity and 140 ± 40 µmol m^{-2} s^{-1} incident photo-irradiance in 20 and 1 L pots for tomato and *N. benthamiana*, respectively.

Because the T0 regenerated plants produced unviable seeds (Supplementary Table S7), transgenic plants, and the corresponding controls, were phenotypically characterized in the first-cutting propagation obtained from T0 plants. The tocopherol deficiency phenotype was confirmed in subsequent cutting experiments (Supplementary Table S8). All assays were performed with 4-8 biological replicates per genotype. Tomato source and sink leaves were sampled from the second and third leaflets of the third totally expanded leaf and of 50 % expanded leaves of 4-week-old plants, respectively. Ripe fruits were collected at 52 days after anthesis. Samples were immediately frozen into liquid N_2, and stored at -80 ºC until further processing.

Six-month-old plants were harvested and fresh aerial biomass was measured for harvest index determination according to the following formula: harvest index = (fruit fresh mass x 100) / total aerial biomass.

Quantitative PCR (qPCR)

RNA extraction, cDNA synthesis and qPCR assays were performed as previously described (Almeida *et al.*, 2016). Primer sequences are listed in Supplementary Table S9. Expression values were normalized against the geometric mean of two reference genes, *CAC* and *EXPRESSED* for fruits and *ELONGATION FACTOR 1-* α (*EF1-*α) for leaves (Quadrana *et al.*, 2013). A permutation test lacking sample distribution assumptions (Pfaffl *et al.*, 2002) was applied to detect statistical differences ($P < 0.05$) in expression ratios using the algorithms in the fgStatistics software package (http://sites.google.com/site/fgStatistics/.)

Cloning procedures

For SlTBP subcellular localization experiments, a fragment of 1,272 spanning the 424 amino acids of the protein was amplified and cloned into pK7FWG2 binary vector (Karimi *et al.*, 2002) using the primers indicated in Supplementary Table S9, resulting in a C-terminal GFP fusion protein (pK7FWG2-SlTBP) (de Godoy *et al.*, 2013). For RNAi silencing, a 224 bp fragment of *SlTBP* gene was used to generate a hairpin construct. To avoid off-target effects the construct was designed to have minimal complementarity with other genes and then, the sense/antisense fragment was used as query for a BLAST search against the Sol Genomics Network database. Six genes matched, only one with more

than 20 nucleotides and none with, at least, 20 consecutive nucleotides. Thus, it is unlikely off-target effects. The fragment was amplified with the primers listed in Supplementary Table S9 and cloned into pK7GWIWG2(I) binary vector (Karimi *et al.*, 2002) to generate a hairpin construct (pK7GWIWG2(I)-SlTBP) (de Godoy *et al.*, 2013). Binary vectors were introduced in *Agrobacterium tumefaciens* strains GV3101 and GV2260 for subcellular localization and plant stable transformation, respectively.

N. benthamiana transient transformation and confocal microscopy

The Agrobacterium strain containing pK7FWG2-SlTBP was grown and infiltrated into leaves of six-week-old *Nicotiana benthamiana* plants (de Godoy *et al.*, 2013). After 48 h, the infiltrated tissues were observed with a confocal laser microscope Zeiss LSM 400 under a 63X water objective. Chlorophyll images were captured over 590 nm after excitation at 543 nm, while the ones for SlTBP::GFP fusion were captured over 505 to 550 nm range after excitation at 488 nm with an argon laser beam.

Plant transformation

Seedling cotyledons of *S. lycopersicum* (cv. Moneymaker) were used as explants to generate transgenic tomato plants with the hairpin construct pK7GWIWG2(I)-SlTBP by Agrobacterium-mediated transformation (Nunes-Nesi *et al.*, 2005). The presence of the transgene was confirmed by PCR with 35S promoter and specific reverse primers (Supplementary Table S9).

Tocopherol and pigment quantification

Tocopherols were extracted and quantified by HPLC (High Performance Liquid Chromatography) (Almeida *et al.*, 2011). Carotenoids and chlorophyll extraction and quantification for leaves were performed according to protocols previously described (Lichtenthaler, 1987). In ripe fruits, β-carotene and lycopene quantification was performed by HPLC (Heredia *et al.*, 2009).

Photosynthetic parameters

Gas exchange and chlorophyll fluorescence parameters were measured in the third fully expanded leaf of 8-week-old plants using a portable open gas-exchange system incorporating infra-red CO_2 and water vapor analyzers (LI-6400XT system; LI-COR) equipped with an integrated modulated chlorophyll fluorometer (LI-6400-40; LI-COR) (de Godoy *et al.*, 2013).

Transmission electron microscopy

Source leaves from three biological replicates of *SlTBP*-knockdown transgenic lines L15 and L24 were fixed, embedded in Spurr resin and ultrathin sections analyzed with a Zeiss EM 900 transmission electron microscope (Lira *et al.*, 2017). For chloroplast and PG counting, and area determination

ImageJ software was used (http://rsb.info.nih.gov/ij/). Pictures of 24 chloroplasts along the tissue were took, 12 close to cuticle and the same number of chloroplasts from fifth cell's layer. All PG inside each chloroplast were counted and measured.

Lipid peroxidation assay

Fresh vegetable material (500 mg for leaves and 1 g for fruits) was homogenized with 5 mL of cold Tris HCl 20 mM pH 4, containing 10 µl of BHT (butylated hydroxytoluene butilado) 0.5 M. TCA was added to 20% final concentration for protein precipitation. After centrifugation for 4 min at 12,000 g, the thiobarbituric acid (TBA) assay was performed in the supernatants as previously described (Heath and Packer, 1968). The malondialdehyde (MDA) equivalent was calculated according to the Lambert and Beer formula: $A = \varepsilon \times \boldsymbol{l} \times \boldsymbol{c}$; where A is the absorbance at 535 nm, ε is the molar extinction coefficient ($1{,}56 \times 10^5$ M cm^{-1}), $\boldsymbol{l}$ is the path length of the cuvette (1 cm) and $\boldsymbol{c}$ is the accurate MDA concentration to be determined.

Lipid profiles

Lipids were extracted from c.a. 50 mg of lyophilized leaf or pericarp, according to (Folch, 1987). Briefly, samples were incubated at 65 °C during 20 min in 2 mL isopropanol. Two mL chloroform and 1 mL H_2O were then added and mix. The organic phase was collected and washed with 1 mL of 1 M KCl. Then, the organic phase was evaporated and lipids were resolubilized with $CHCl_3$:MeOH (2:1, v:v). Lipids were then deposed by Linomat 5 (Camag) onto silica plates separated by thin layer chromatography (TLC) in parallel with lipid standards, using Vitiello-Zanetta solvent mixture (Deranieh *et al.*, 2013) or Juguelin one (Juguelin *et al.*, 1986) for polar or neutral lipids respectively. Lipids were revealed by exposition under UV illumination after incubation of the plates in a solution of 0.001% (w/v) primuline. The areas on the silica plates corresponding to the different lipid classes were scrapped separately and incubated with 1 mL of MeOH, 2.5% H_2SO_4 (v/v) and C17:0 at 5 µg/mL as internal standard in hermetically closed tubes for 1 h at 80 °C. Fatty acid methyl esters (FAMEs) were then extracted in 400 µL hexane and analyzed by Gas Chromatography performed using an Agilent 7890 gas chromatograph equipped with a Carbowax column (15 m x 0.53 mm, 1.2 µm; Alltech Associates, Deerfield, IL, USA) and flame ionization detection. The temperature gradient was 160 °C for 1 min, increased to 190 °C at 20 °C/min, increased to 210 °C at 5 °C/min and then remained at 210 °C for 5 min. FAMES were identified by comparing their retention times with commercial fatty acid standards (Sigma-Aldrich) and quantified using ChemStation (Agilent) to calculate the peak surfaces, and then comparing them with the C17:0 response.

Microarray hybridization

Gene expression was profiled by microarray from three biological replicates of L15, L18 L24 and control plants for leaves and ripe fruits organs. Each replicate was composed by a pool of samples

collected from two plants. RNA pools (1 µg of each genotype) were amplified and aminoallyl labeled using the MessageAmp II aRNA kit (Ambion) and 5-(3-aminoallyl)-2'-deoxyuridine-5'-triphosphate following the manufacturer's instructions.). Ten µg of aminoallyl-labeled amplified RNA was used to label with Cy5 (Reactive Dye Pack; Amersham). An equal quantity of control RNA pool was labeled with Cy3. Equal mixtures of labeled RNA were hybridized to tomato long-mer oligoarray (70 bp) slides (Microarrays Inc.) representing 12,160 genes. Hybridizations were carried out in 100 µL of hybridization solution (5 x SSC, 0.1% SDS, 40% formamide) containing 100 ρmol of Cy3- and Cy5-labelled samples and incubated at 42 ºC on a thermal bath for 16 h. Then the slides were washed with 2 x SSC 0.1% SDS 4 times for 10 min. Six additional washes (three with 0.1 x SSC 0.1% SDS and three with 0.1 x SSC, for 10 min each) at room temperature were performed before drying the glass slides with a brief centrifugation. Slides were scanned at 532 and 635 nm with a ScanArray Gx scanner at 10 µm resolution, 90% laser power and different photomultiplicator values to adjust the ratio intensity to 1.0. Raw signal intensity values were computed from the scanned array images using the image analysis software ScanArray Express (Pelkin Elmer). File data were analysed by the Robin software package (Lohse *et al.*, 2010) using default settings for two-color microarray analysis. Briefly, intensity raw data were collected background-subtracted, normalized within each array by the print tip-wise normalization method (Yang *et al.*, 2002), and subsequently scaled across all arrays to have the same median absolute deviation (Yang *et al.*, 2002; Smyth and Speed, 2003). To detect differentially expressed genes, a linear model-based approach (Smyth, 2004) was applied to compare the mean normalized values for a gene between experimental groups (transgenic and control). Mean values of differential genes were calculated from each sample as log2 values. A gene was considered differentially expressed (DEG) when its mRNA accumulation was different than control genotype in the same direction (up- or down-regulated) in at least two transgenic lines either by *P* value ($P < 0.05$) or Log fold change (>1.0 or < -1.0). Distribution of DEG within the three analysed *SlTBP*-knockdown lines is shown in Supplementary Figure S5. Functional categorization of DEG was performed using the MapMan software (Thimm *et al.*, 2004).

Starch quantification

Starch content was spectrophotometrically determined in T0 generation transgenic lines (Dominguez *et al.*, 2013).

Polar metabolite profiles

Extraction, derivatization, standard addition, and sample injection for GC-MS were performed as previously described (Lisec *et al.*, 2006),(Osorio *et al.*, 2012). Identification and quantification of the compounds were performed with TagFinder 4.0 software and the mass spectra were cross-referenced with those in the Golm Metabolome Database (Schauer *et al.*, 2005; Kopka *et al.*, 2005). Three to six biological replicates were used for this analysis.

Data analyses

Differences in parameters were analysed using Infostat software version 2011 (http://www.infostat.com.ar). When the data set showed homoscedasticity, ANOVA – Tukey test ($P < 0.05$) was performed to compare transgenic lines against the control genotype. In the absence of homoscedasticity, a non-parametric comparison was performed by applying the Kruskal Wallis test ($P < 0.05$). All values represent the mean of at least three biological replicates. A parameter was considered to be affected by *SlTBP* silencing if at least 50% of the tested *SlTBP*-knockdown lines differed significantly from the wild type genotype in the same direction.

ACKNOWLEDGEMENTS

This work was supported by Fundação de Amparo à Pesquisa do Estado de São Paulo (Brazil; FAPESP 2010-50535-0), Conselho Nacional de Desenvolvimento Científico e Tecnológico (CNPq, Brazil), Coordenação de Aperfeiçoamento de Pessoal de Nível Superior (CAPES, Brazil), Universidade de São Paulo (USP, Brazil), Instituto Nacional de Tecnología Agropecuaria (INTA, Argentina), Fondo para la Investigación Científica y Tecnológica (FONCYT, Argentina) and Consejo Nacional de Investigaciones Científicas y Técnicas (CONICET, Argentina), Fondo de Financiamiento de Centros de Investigación en Áreas Prioritarias (FONDAP 15090007, Chile), Fondo Nacional de Desarrollo Científico y Tecnológico (Fondecyt 11160899, (Chile), The Novo Nordisk Foundation (Biotechnology-based Synthesis and Production Research), The Villum Foundation (PLANET project), the Danish Agency for Science, Technology and Innovation (Danish-Brazilian Network for Plant Glycoscience) and from the MINCYT-ECOS program (Argentina-France). L.B., B.S.L., F.G. and J.A. were recipients of FAPESP fellowships. L.B., M.R., and D.D. were funded by a fellowship from CNPq. L.B., R.A. and F.C. are members of the Argentine Council of Science and Technology (CONICET). Imaging was performed at the Bordeaux Imaging Center, member of the national infrastructure France BioImaging. The help of B. Batailler is acknowledged.

CONFLICTS OF INTEREST

The authors declare no conflicts of interest.

SUPPORTING INFORMATION

Additional Supporting information may be found in the online version of this article.

Supplementary Table S1. Diversity of SEC14-related proteins.

Supplementary Table S2. Metabolite profiles of *SlTBP*-knockdown lines.

Supplementary Table S3. Yield parameters of *SlTBP*-knockdown lines.

Supplementary Table S4. Lipid profiles of *SlTBP*-knockdown lines.

Supplementary Table S5. Differentially expressed genes of *SlTBP*-knockdown lines.

Supplementary Table S6. Validation of differentially expressed genes by qPCR.

Supplementary Table S7. Germination assays for T1 SlSBP-lines.

Supplementary Table S8. Tocopherol contents in the third-cutting experiment of SlTBP-knockdown lines.

Supplementary Table S9. Primers used in the experiments.

Supplementary Figure S1. Structural similarities between SlTBP and HsTTP.

Supplementary Figure S2. SlTBP MALDI mass spectrometry.

Supplementary Figure S3. *SlTBP*-knockdown effectiveness.

Supplementary Figure S4. Lipid peroxidation in fruits of *SlTBP*-knockdown lines.

Supplementary Figure S5. Genes with altered transcriptional profile in at least two *SlTBP*-knockdown lines.

Supplementary Figure S6. Differentially expressed genes in source leaves and ripe fruits from *SlTBP*-silenced plants.

Supplementary Figure S7. Spectroscopic characterization of tocopherol-biotin conjugate.

REFERENCES

Almeida, J., Quadrana, L., Asís, R., Setta, N., de Godoy, F., Bermúdez, L., et al. (2011) Genetic dissection of vitamin E biosynthesis in tomato. *J. Exp. Bot.*, 62, 3781–98.

Almeida, J., Silva Azevedo, M. Da, Spicher, L., Glauser, G., vom Dorp, K., Guyer, L., et al. (2016) Down-regulation of tomato PHYTOL KINASE strongly impairs tocopherol biosynthesis and affects prenyllipid metabolism in an organ-specific manner. *J. Exp. Bot.*, 67, 919–934.

Anantharaman, V. and Aravind, L. (2002) The GOLD domain, a novel protein module involved in Golgi function and secretion. *Genome Biol.*, 3, research0023.

Andrews, P.K., Fahy, D.A. and Foyer, C.H. (2004) Relationships between fruit exocarp antioxidants in the tomato (Lycopersicon esculentum) high pigment-1 mutant during development. *Physiol. Plant.*, 120, 519–528.

Auldridge, M.E., Block, A., Vogel, J.T., Dabney-Smith, C., Mila, I., Bouzayen, M., et al. (2006) Characterization of three members of the Arabidopsis carotenoid cleavage dioxygenase family demonstrates the divergent roles of this multifunctional enzyme family. *Plant J.*, 45, 982–993.

Austin, J.R. (2006) Plastoglobules Are Lipoprotein Subcompartments of the Chloroplast That Are Permanently Coupled to Thylakoid Membranes and Contain Biosynthetic Enzymes. *Plant Cell Online*, 18, 1693–1703.

Bankaitis, V.A., Mousley, C.J. and Schaaf, G. (2010) The Sec14-superfamily and mechanisms for crosstalk between lipid metabolism and lipid signaling. *Trends Biochem. Sci.*, 35, 150–160.

Biasini, M., Bienert, S., Waterhouse, A., Arnold, K., Studer, G., Schmidt, T., et al. (2014) SWISS-MODEL: modelling protein tertiary and quaternary structure using evolutionary information. *Nucleic Acids Res.*, 42, W252–W258.

Castro, E. de, Sigrist, C.J.A., Gattiker, A., Bulliard, V., Langendijk-Genevaux, P.S., Gasteiger, E., et al. (2006) ScanProsite: detection of PROSITE signature matches and ProRule-associated functional and structural residues in proteins. *Nucleic Acids Res.*, 34, W362–W365.

Deranieh, R.M., Joshi, A.S. and Greenberg, M.L. (2013) Thin-layer chromatography of phospholipids. *Methods Mol. Biol.*, 1033, 21–27.

Dereeper, A., Guignon, V., Blanc, G., et al. (2008) Phylogeny.fr: robust phylogenetic analysis for the non-specialist. *Nucleic Acids Res.*, 36, W465–W469.

Dominguez, P.G., Frankel, N., Mazuch, J., Balbo, I., Iusem, N., Fernie, A.R., et al. (2013) ASR1 Mediates Glucose-Hormone Cross Talk by Affecting Sugar Trafficking in Tobacco Plants. *Plant Physiol.* , 161, 1486–1500.

Dorp, K. vom, Hölzl, G., Plohmann, C., Eisenhut, M., Abraham, M., Weber, A.P.M., et al. (2015) Remobilization of Phytol from Chlorophyll Degradation Is Essential for Tocopherol Synthesis and Growth of Arabidopsis. *Plant Cell*, tpc.15.00395.

Dudareva, N., Martin, D., Kish, C.M., Kolosova, N., Gorenstein, N., Fäldt, J., et al. (2003) (E)-β-Ocimene and Myrcene Synthase Genes of Floral Scent Biosynthesis in Snapdragon: Function and Expression of Three Terpene Synthase Genes of a New Terpene Synthase Subfamily. *Plant Cell*, 15, 1227–1241.

Emanuelsson, O., Nielsen, H. and Heijne, G. von (1999) ChloroP, a neural network-based method for predicting chloroplast transit peptides and their cleavage sites. *Protein Sci.*, 8, 978–84.

Folch (1987) A simple method for the isolation and purification of total lipides from animal tissues. *J. Biol. Chem.*, 55, 999–1033.

Foyer, C.H. and Shigeoka, S. (2011) Understanding Oxidative Stress and Antioxidant Functions to Enhance Photosynthesis. *Plant Physiol.*, 155, 93–100.

Giovannoni, J., Nguyen, C., Ampofo, B., Zhong, S. and Fei, Z. (2017) The Epigenome and Transcriptional Dynamics of Fruit Ripening. *Annu. Rev. Plant Biol*. 68:61–84.

Godoy, F. de, Bermudez, L., Lira, B.S., de Souza, A. P., Elbl, P., Demarco, D., et al. (2013) Galacturonosyltransferase 4 silencing alters pectin composition and carbon partitioning in tomato. *J. Exp. Bot.*, 64, 2449–2466.

Gonzalez-Jorge, S., Ha, S.-H., Magallanes-Lundback, M., Gilliland, L. U., Zhou, A., Lipka, A. E., et al. (2013) CAROTENOID CLEAVAGE DIOXYGENASE4 Is a Negative Regulator of β-Carotene Content in Arabidopsis Seeds. *Plant Cell*, 25, 4812–4826.

Guindon, S., Dufayard, J.-F., Lefort, V., Anisimova, M., Hordijk, W. and Gascuel, O. (2010) New Algorithms and Methods to Estimate Maximum-Likelihood Phylogenies: Assessing the Performance of PhyML 3.0. *Syst. Biol.*, 59, 307–321.

Havaux, M., Dall'Osto, L. and Bassi, R. (2007) Zeaxanthin Has Enhanced Antioxidant Capacity with Respect to All Other Xanthophylls in Arabidopsis Leaves and Functions Independent of Binding to PSII Antennae. *Plant Physiol.*, 145, 1506–1520.

Havaux, M., Eymery, F., Porfirova, S., Rey, P. and Dörmann, P. (2005) Vitamin E protects against photoinhibition and photooxidative stress in Arabidopsis thaliana. *Plant Cell*, 17, 3451–3469.

Heath, R.L. and Packer, L. (1968) Photoperoxidation in isolated chloroplasts: I. Kinetics and stoichiometry of fatty acid peroxidation. *Arch. Biochem. Biophys.*, 125, 189–198.

Heredia, A., Peinado, I., Barrera, C. and Grau, A.A. (2009) Influence of process variables on colour changes, carotenoids retention and cellular tissue alteration of cherry tomato during osmotic dehydration. *J. Food Compos. Anal.*, 22, 285–294.

Hölscher, C., Meyer, T. and Schaewen, A. Von (2014) Dual-targeting of arabidopsis 6-

phosphogluconolactonase 3 (PGL3) to chloroplasts and peroxisomes involves interaction with Trx m2 in the cytosol. *Mol. Plant*, 7, 252–255.

Jones, P., Binns, D., Chang, H.-Y., Fraser, M., Li, W., McAnulla, C., et al. (2014) InterProScan 5: genome-scale protein function classification. *Bioinformatics*, 30, 1236–1240.

Juguelin, H., Heape, A., Boiron, F. and Cassagne, C. (1986) A quantitative developmental study of neutral lipids during myelinogenesis in the peripheral nervous system of normal and trembler mice. *Dev. Brain Res.*, 25, 249–252.

Karimi, M., Inzé, D. and Depicker, A. (2002) GATEWAY^{TM} vectors for Agrobacterium-mediated plant transformation. *Trends Plant Sci.*, 7, 193–195.

Keim, V., Manzano, D., Fernández, F.J., Closa, M., Andrade, P., Caudepón, D., et al. (2012) Characterization of Arabidopsis FPS Isozymes and FPS Gene Expression Analysis Provide Insight into the Biosynthesis of Isoprenoid Precursors in Seeds J. L. Heazlewood, ed. *PLoS One*, 7, e49109.

Kelley, L.A., Mezulis, S., Yates, C.M., Wass, M.N. and Sternberg, M.J.E. (2015) The Phyre2 web portal for protein modelling, prediction and analysis. *Nat. Protoc.*, 10, 845–858.

KF de Campos, M. and Schaaf, G. (2017) The regulation of cell polarity by lipid transfer proteins of the SEC14 family. *Curr. Opin. Plant Biol.*, 40, 158–168.

Kono, N., Ohto, U., Hiramatsu, T., Urabe, M., Uchida, Y., Satow, Y., et al. (2013) Impaired -TTP-PIPs Interaction Underlies Familial Vitamin E Deficiency. *Science*, 340, 1106–1110.

Kopka, J., Schauer, N., Krueger, S., Birkemeyer, C., Usadel, B., Bergmüller, E., et al. (2005) GMD@CSB.DB: the Golm Metabolome Database. *Bioinformatics*, 21, 1635–1638.

Krieger-Liszkay, A. and Trebst, A. (2006) Tocopherol is the scavenger of singlet oxygen produced by the triplet states of chlorophyll in the PSII reaction centre. *J. Exp. Bot.*, 57, 1677–84.

Li-Beisson, Y., Shorrosh, B., Beisson, F., Andersson, M. X., Arondel, V., Bates, P. D., et al. (2010) Acyl-Lipid Metabolism. *Arabidopsis Book*, 8, e0133.

Lichtenthaler, H.K.B.T.-M. in E. (1987) [34] Chlorophylls and carotenoids: Pigments of photosynthetic biomembranes. In *Plant Cell Membranes*. Academic Press, pp. 350–382.

Lippold, F., Dorp, K. vom, Abraham, M., Hölzl, G., Wewer, V., Yilmaz, J. L., et al. (2012) Fatty Acid Phytyl Ester Synthesis in Chloroplasts of Arabidopsis. *Plant Cell*, 24, 2001–2014.

Lira, B.S., Gramegna, G., Trench, B., Alves, F. R. R., Silva, É. M., Silva, G. F. F., et al. (2017) Manipulation of a senescence-associated gene improves fleshy fruit yield. *Plant Physiol.*, 175:77-91.

Lisec, J., Schauer, N., Kopka, J., Willmitzer, L. and Fernie, A.R. (2006) Gas chromatography mass spectrometry-based metabolite profiling in plants. *Nat. Protoc.*, 1, 387–396.

Löbbecke, L. and Cevc, G. (1995) Effects of short-chain alcohols on the phase behavior and interdigitation of phosphatidylcholine bilayer membranes. *Biochim. Biophys. Acta - Biomembr.*, 1237, 59–69.

Lohse, M., Nunes-Nesi, A., Krüger, P., Nagel, A., Hannemann, J., Giorgi, F. M., et al. (2010) Robin: An Intuitive Wizard Application for R-Based Expression Microarray Quality Assessment and Analysis. *Plant Physiol.*, 153, 642 LP-651.

Maeda, H., Sage, T.L., Isaac, G., Welti, R. and DellaPenna, D. (2008) Tocopherols Modulate Extraplastidic Polyunsaturated Fatty Acid Metabolism in Arabidopsis at Low Temperature. *Plant Cell Online*, 20, 452–470.

Mehrshahi, P., Johnny, C. and DellaPenna, D. (2014) Redefining the metabolic continuity of chloroplasts and ER. *Trends Plant Sci.*, 19, 501–507.

Mehrshahi, P., Stefano, G., Andaloro, J.M., Brandizzi, F., Froehlich, J.E. and DellaPenna, D. (2013) Transorganellar complementation redefines the biochemical continuity of endoplasmic reticulum and chloroplasts. *Proc. Natl. Acad. Sci.*, 110, 12126–12131.

Meier, R., Tomizaki, T., Schulze-Briese, C., Baumann, U. and Stocker, A. (2003) The Molecular Basis of Vitamin E Retention: Structure of Human α-Tocopherol Transfer Protein. *J. Mol. Biol.*, 331, 725–734.

Miller, M.B., Vishwanatha, K.S., Mains, R.E. and Eipper, B.A. (2015) An N-terminal Amphipathic Helix Binds Phosphoinositides and Enhances Kalirin Sec14 Domain-mediated Membrane Interactions. *J. Biol. Chem.*, 290, 13541–13555.

Min, K.C., Kovall, R.A. and Hendrickson, W.A. (2003) Crystal structure of human α-tocopherol transfer protein bound to its ligand: Implications for ataxia with vitamin E deficiency. *Proc. Natl. Acad. Sci. U. S. A.*, 100, 14713–14718.

Miret, J. a and Munné-Bosch, S. (2015) Redox signaling and stress tolerance in plants: a focus on vitamin E. *Ann. N. Y. Acad. Sci.*, 1–10.

Nacir, H. and Bréhélin, C. (2013) When proteomics reveals unsuspected roles: the plastoglobule example. *Front. Plant Sci.*, 4, 114.

Nava, P., Cecchini, M., Chirico, S., Gordon, H., Morley, S., Manor, D., et al. (2006) Preparation of fluorescent tocopherols for use in protein binding and localization with the alpha-tocopherol transfer protein. *Bioorg. Med. Chem.*, 14, 3721–3736.

Nunes-Nesi, A., Carrari, F., Lytovchenko, A., Smith, A.M.O., Loureiro, M.E., Ratcliffe, R.G., et al. (2005) Enhanced photosynthetic performance and growth as a consequence of decreasing mitochondrial malate dehydrogenase activity in transgenic tomato plants. *Plant Physiol.*, 137, 611–22.

Osorio, S., Do, P.T. and Fernie, A.R. (2012) Plant Metabolomics. , 860, 101–109. Available at: http://link.springer.com/10.1007/978-1-61779-594-7.

Padham, A.K., Hopkins, M.T., Wang, T.-W., McNamara, L.M., Lo, M., Richardson, L.G.L., Smith, M.D., Taylor, C.A. and Thompson, J.E. (2007) Characterization of a Plastid Triacylglycerol Lipase from Arabidopsis. *Plant Physiol.*, 143, 1372-1384.

Panagabko, C., Morley, S., Hernandez, M., Cassolato, P., Gordon, H., Parsons, R., et al. (2003) Ligand Specificity in the CRAL-TRIO Protein Family. *Biochemistry*, 42, 6467–6474.

Pellaud, S. and Mène Saffrané, L. (2017) Metabolic Origins and Transport of Vitamin E Biosynthetic Precursors. *Front. Plant Sci*. 8, 1959.

Peterman, T.K. (2004) Patellin1, a Novel Sec14-Like Protein, Localizes to the Cell Plate and Binds Phosphoinositides. *Plant Physiol.*, 136, 3080–3094.

Peterman, T.K., Ohol, Y.M., Mcreynolds, L.J., Luna, E.J., Sciences, B., College, W., et al. (2004)

Patellin1 , a Novel Sec14-Like Protein , Localizes to the Cell Plate and Binds Phosphoinositides 1. *Society*, 136, 1–15.

Peterman, T.K., Sequeira, A.S., Samia, J. a and Lunde, E.E. (2006) Molecular cloning and characterization of patellin1, a novel sec14-related protein, from zucchini (Cucurbita pepo). *J. Plant Physiol.*, 163, 1150–8.

Pfaffl, M.W., Horgan, G.W. and Dempfle, L. (2002) Relative expression software tool (REST) for group-wise comparison and statistical analysis of relative expression results in real-time PCR. *Nucleic Acids Res.*, 30, e36.

Quadrana, L., Almeida, J., Asís, R., Duffy, T., Dominguez, P. G., Bermúdez, L., et al. (2014) Natural occurring epialleles determine vitamin E accumulation in tomato fruits. *Nat. Commun.*, 5, 4027.

Quadrana, L., Almeida, J., Otaiza, S.N., Duffy, T., Da Silva, J. V. C., de Godoy, F., et al. (2013) Transcriptional regulation of tocopherol biosynthesis in tomato. *Plant Mol. Biol.*, 81, 309–25.

Saito, K., Tautz, L. and Mustelin, T. (2007) The lipid-binding SEC14 domain. *Biochim. Biophys. Acta - Mol. Cell Biol. Lipids*, 1771, 719–726.

Schaaf, G., Ortlund, E.A., Tyeryar, K.R., Mousley, C. J., Ile, K. E., Garrett, T. A., et al. (2008) Functional Anatomy of Phospholipid Binding and Regulation of Phosphoinositide Homeostasis by Proteins of the Sec14 Superfamily. *Mol. Cell*, 29, 191–206.

Schauer, N., Semel, Y., Roessner, U., Gur, A., Balbo, I., Carrari, F., et al. (2006) Comprehensive metabolic profiling and phenotyping of interspecific introgression lines for tomato improvement. *Nat. Biotechnol.*, 24, 447–54.

Schauer, N., Zamir, D. and Fernie, A.R. (2005) Metabolic profiling of leaves and fruit of wild species tomato: a survey of the Solanum lycopersicum complex. *J. Exp. Bot.*, 56, 297–307.

Sikkema, J., Bont, J.A. de and Poolman, B. (1995) Mechanisms of membrane toxicity of hydrocarbons. *Microbiol. Rev.*, 59, 201–222.

Simkin, A.J., Underwood, B.A., Auldridge, M., Loucas, H.M., Shibuya, K., Schmelz, E., et al. (2004) Circadian Regulation of the PhCCD1 Carotenoid Cleavage Dioxygenase Controls Emission of b - Ionone , a Fragrance Volatile of Petunia Flowers 1. , 136, 3504–3514.

Smyth, G.K. (2004) Linear Models and Empirical Bayes Methods for Assessing Differential Expression in Microarray Experiments. *Stat. Appl. Genet. Mol. Biol.*, 3, 1–25.

Smyth, G.K. and Speed, T. (2003) Normalization of cDNA microarray data. *Methods*, 31, 265–273.

Song, W., Maeda, H. and DellaPenna, D. (2010) Mutations of the ER to plastid lipid transporters TGD1, 2, 3 and 4 and the ER oleate desaturase FAD2 suppress the low temperature-induced phenotype of Arabidopsis tocopherol-deficient mutant vte2. *Plant J.*, 62, 1004–1018.

Spicher, L. Almeida J., Gutbrod K., Pipitone R., Dörmann P., Glauser G., et al. (2017) Essential role for phytol kinase and tocopherol in tolerance to combined light and temperature stress in tomato. *J. Exp. Bot.* Available at: doi:10.1093/jxb/erx356.

Spicher, L. and Kessler, F. (2015) Unexpected roles of plastoglobules (plastid lipid droplets) in vitamin K and E metabolism. *Curr. Opin. Plant Biol.*, 25, 123–129.

Stevenson, J.M., Perera, I.Y., Heilmann, I., Persson, S. and Boss, W.F. (2000) Inositol signaling and plant growth. *Trends Plant Sci.*, 5, 252–258.

Stocker, A. and Baumann, U. (2003) Supernatant protein factor in complex with RRR-alpha-tocopherylquinone: a link between oxidized Vitamin E and cholesterol biosynthesis. *J. Mol. Biol.*, 332, 759–65.

Suzuki, T., Matsushima, C., Nishimura, S., Higashiyama, T., Sasabe, M. and Machida, Y. (2016) Identification of Phosphoinositide-Binding Protein PATELLIN2 as a Substrate of Arabidopsis MPK4 MAP Kinase during Septum Formation in Cytokinesis. , 57, 1744–1755.

Tamura, K., Stecher, G., Peterson, D., Filipski, A. and Kumar, S. (2013) MEGA6: Molecular Evolutionary Genetics Analysis Version 6.0. *Mol. Biol. Evol.*, 30, 2725–2729.

Tanksley, S.D. (2004) The Genetic , Developmental , and Molecular Bases of Fruit Size and Shape Variation in Tomato. *Nature*, 16, 181–189.

Thimm, O., Bläsing, O., Gibon, Y., Nagel, A., Meyer, S., Krüger, P., et al. (2004) MAPMAN: a user-driven tool to display genomics data sets onto diagrams of metabolic pathways and other biological processes. *Plant J.*, 37, 914–939.

Valentin, H.E. (2006) The Arabidopsis vitamin E pathway gene5-1 Mutant Reveals a Critical Role for Phytol Kinase in Seed Tocopherol Biosynthesis. *Plant Cell Online*, 18, 212–224.

Vidi, P.-A., Kanwischer, M., Baginsky, S., Austin, J.R., Csucs, G., Dörmann, P., et al. (2006) Tocopherol cyclase (VTE1) localization and vitamin E accumulation in chloroplast plastoglobule lipoprotein particles. *J. Biol. Chem.*, 281, 11225–34.

Yang, W., Wang, G., Li, J., Bates, P.D., Wang, X. and Allen, D.K. (2017) Phospholipase Dζ Enhances Diacylglycerol Flux into Triacylglycerol. *Plant Physiol.*, 174, 110–123.

Yang, Y.H., Dudoit, S., Luu, P., Lin, D.M., Peng, V., Ngai, J., et al. (2002) Normalization for cDNA microarray data: a robust composite method addressing single and multiple slide systematic variation. *Nucleic Acids Res.*, 30, e15–e15.

Table 1. Pigment and tocopherol contents in *SlTBP*-knockdown lines.

Source leaves					
	WT	**L15**	**L18**	**L19**	**L24**
Chlorophyll *a* †	111.59 ± 4.86	116.55 ± 10.81	114.95 ± 7.58	115.26 ± 9.39	99.09 ± 6.01
Chlorophyll *b* †	31.30 ± 1.97	34.97 ± 3.58	33.37 ± 2.10	34.06 ± 2.73	27.08 ± 1.97
Total carotenoids †	31.69 ± 1.32	35.22 ± 2.95	33.76 ± 2.11	26.95 ± 4.18	29.71 ± 1.85
α-tocopherol ‡	50.57 ± 2.03	**28.18 ± 9.08**	**41.02 ± 8.54**	**47.2 ± 0.48**	**38.67 ± 5.37**
ɣ-tocopherol ‡	3.35 ± 1.58	**1.00 ± 0.26**	2.75 ± 0.91	**1.44 ± 0.12**	**1.32 ± 0.40**
Total-tocopherol ‡	55.64 ± 4.67	**29.85 ± 10.24**	**44.44 ± 9.74**	**48.67 ± 0.42**	**40.11 ± 5.30**
Ripe fruits					
	WT	**L15**	**L18**	**L19**	**L24**
β-carotene §	0.30 ± 0.06	**0.12 ± 0.01**	**0.08 ± 0.01**	**0.07 ± 0.01**	**0.07 ± 0.02**
Lycopene §	20.82 ± 3.57	11.28 ± 1.39	**8.54 ± 0.47**	**6.84 ± 1.84**	**8.89 ± 0.18**
α-tocopherol ‡	17.72 ± 3.75	18.1 ± 0.33	14.66 ± 5.09	13.69 ± 2.05	**11.89 ± 1.82**
β-tocopherol ‡	0.21 ± 0.01	**0.27 ± 0.02**	0.22 ± 0.02	0.19 ± 0.04	0.20 ± 0.01
ɣ-tocopherol ‡	4.35 ± 0.75	4.14 ± 1.47	**2.94 ± 0.73**	**2.31 ± 0.10**	**3.05 ± 0.17**
δ-tocopherol ‡	0.13 ± 0.02	0.29 ± 0.13	**0.09 ± 0.01**	0.08 ± 0.06	0.16 ± 0.03
Total-tocopherol ‡	22.05 ± 4.49	23.52 ± 2.48	17.45 ± 6.22	**16.28 ± 2.05**	**15.3 ± 1.95**

Values are represented as means ± SD of at least three biological replicates. Values in bold denote significant differences between the wild-type (WT) and *SlTBP*-knockdown genotypes ($P < 0.05$). †μg/cm^2; ‡μg/g fresh weight; §mg/100 g fresh weight.

Table 2. Gas-exchange and chlorophyll fluorescence parameters in *SlTBP*-knockdown lines.

	WT	L15	L18	L19	L24
qP	0.58 ± 0.01	**0.52 ± 0.02**	**0.50 ± 0.02**	**0.52 ± 0.03**	**0.53 ± 0.03**
NPQ	1.42 ± 0.09	**1.64 ± 0.11**	**1.57 ± 0.10**	**1.58 ± 0.12**	**1.56 ± 0.10**
ETR	148.70 ± 6.42	**131.10 ± 9.23**	**126.50 ± 7.17**	144.10 ± 6.14	**133.70 ± 8.15**
1-pQ	0.43 ± 0.01	**0.49 ± 0.03**	**0.50 ± 0.02**	0.44 ± 0.02	**0.47 ± 0.03**
Φ_{PSII}	0.29 ± 0.01	**0.25 ± 0.02**	**0.23 ± 0.02**	**0.25 ± 0.02**	**0.24 ± 0.02**
A	10.42 ± 1.79	7.94 ± 2.32	9.19 ± 1.89	10.51 ± 1.89	8.55 ± 1.89
gs	0.07 ± 0.02	0.06 ± 0.01	0.09 ± 0.02	**0.14 ± 0.02**	0.08 ± 0.03
E	1.63 ± 0.45	1.80 ± 0.21	2.19 ± 0.3	**3.09 ± 0.31**	1.77 ± 0.47

qP=[(Fm'-Fs)/(Fm'-F0')], photochemical quenching; NPQ=[(Fm -Fm')/Fm'], non photochemical quenching; ETR=[(Fm'–Fs)/Fm']xfIαleaf, electron transport rate; 1-pQ=[(Fs-F0')/(Fm'-F0')], reduced plastoquinones; Φ_{PSII}=[(Fm'-Fs)/Fm'], PSII operating efficiency; *A* (μmol CO_2 m^{-2} s^{-1}), CO_2 assimilation rate; *gs* (mmol $H_2O.m^{-2}.s^{-1}$), leaf stomatal conductance; *E* (mmol $H_2O.m^{-2}.s^{-1}$), transpiration rate. Data correspond to measurements in the third fully expanded leaf of 8-week-old plants and represent the means ± SD of six biological replicates. Values in bold denote significant differences between the wild-type (WT) and *SlTBP*-knockdown genotypes ($P < 0.05$).

FIGURE LEGENDS

Fig. 1 Characterization of SEC14-like proteins.

A Phylogenetic reconstruction of SEC14-like proteins. Sequences were identified in Phytozome and NCBI database (Supplementary Table S1). Representative protein structures for each clade are outlined on the right showing the domains: CRAL-TRIO N terminal (IPR011074), CRAL-TRIO domain (IPR001251), and GOLD domain (IPR009038). Chloroplast signal peptide was identified by ChloroP software prediction (Emanuelsson *et al.*, 1999) . SlTBP containing clade is highlighted in green.

B Detail of the AtPATL6/SlTBP-like clade. Sequences highlighted with circles are predicted to be targeted to plastids.

C Transient expression of SlTBP::GFP fusion protein in mesophyll cells of *Nicotiana benthamiana* leaves indicates chloroplast targeting under confocal microscopy examination. Chlorophyll autofluorescence, GFP fluorescece and merged signals are indicated above the panels.

D *SlTBP* gene transcript profile in leaves and fruits. Data indicates relative expression normalized against ripe stage. Data represent mean ± SE from at least three biological replicates. Letters indicate statistically different values ($P < 0.05$). SiL, sink leaf; SoL, source leaf; G, green fruit stage; MG, mature green fruit stage; Br, breaker fruit stage; R, ripe fruit stage.

Fig. 2 Heterologous expression of SlTBP protein and binding assays.

A Western blot (WB) and Ponceau staining (PS) of SlTBP-His protein expressed in *Escherichia coli* (BL21AI strain). Western Blot was performed using an anti-His antibody. Lanes 1 and 3: total protein extract from two independent *E. coli* clones expressing the SlTBP; Lane 2: negative control; total protein extract from an untransformed *E. coli* clone. Arrow indicates SlTBP protein.

B Coomasie blue stained gel from affinity chromatography assay showing SlTBP binding to α-tocopherol from *E. coli* extract. B: breakthrough; W: washing steps as detailed in material and method section; E: elution with α-tocopherol. Arrow indicates SlTBP protein as confirmed by MALDI Mass Spectrometry (Supplementary Figure S2).

C Coomasie blue stained gel from affinity chromatography assays showing purified SlTBP binding to α-tocopherol (above) and phylloquinone (below). B: breakthrough; W: washing steps as detailed in Material and Method section; T: elution with α-tocopherol; K: elution with phylloquinone. Arrow indicates SlTBP protein.

Fig. 3 Primary metabolic profile of *SlTBP*-knockdown lines. SoL, source leaves; R, ripe fruits. Data were normalized to fresh weight and presented as the Log_2 ratio between *SlTBP*-knockdown plants and WT. All the ratio values are shown in Supplementary Table S2. Only statistically significant values compared to the wild type genotype are shown in the colour gradient ($P < 0.05$). Gray colour indicates non-detected.

Fig. 4 Lipid peroxidation, chloroplast structure and lipid profile of *SlTBP*-knockdown lines.

A Lipid peroxidation assay in leaves. Values represent means ± SE of at least three biological replicates. Asterisks denote statistically significant values compared to the wild type (WT) genotype ($P < 0.05$).

B Chloroplast structure of wild type (WT) and *SlTBP*-knockdown leaves. G, grana; S, starch granule; LD, lipid droplet; PG, plastoglobule.

C Chloroplast and plastoglobuli (PG) size, ratio and area. Values represent means ± SE of at least three biological replicates. Asterisks denote statistically significant values compared to the wild type (WT) genotype ($P < 0.05$).

D Content of the main lipid classes. MGDG: monogalactosyldiacyl glycerols; DGDG: digalactosyldiacyl glycerols; NL: total neutral lipids (fatty acid phytyl esters, triacylglycerides, free fatty acids and diacylglycerols); PL: total phospholipids (phosphatidyl glycerols, phosphatidyl ethanolamines, phosphatidic acids, phosphatidyl inositols, phosphatidyl cholines). Values represent means ± SE of at least three biological replicates. Asterisks denote statistically significant values compared to the wild type (WT) genotype ($P < 0.05$).

Fig. 5 Differentially expressed genes in leaves (**A**) and ripe fruits (**B**) from *SlTBP*-knockdown lines. The numbers refer to differentially expressed genes (Supplementary Table S5) within the following selected categories: photosynthesis, tetrapyrrole synthesis, lipid metabolism, isoprenoid metabolism, inositol/phosphoinositides metabolism, redox homeostasis. Ch: chloroplast, Chr: chromoplast, ER: endoplasmic reticulum, Vac: vacuole, Cyt: cytosol, PM: plasma membrane. Red and blue squares represent up and down-regulated genes, respectively.

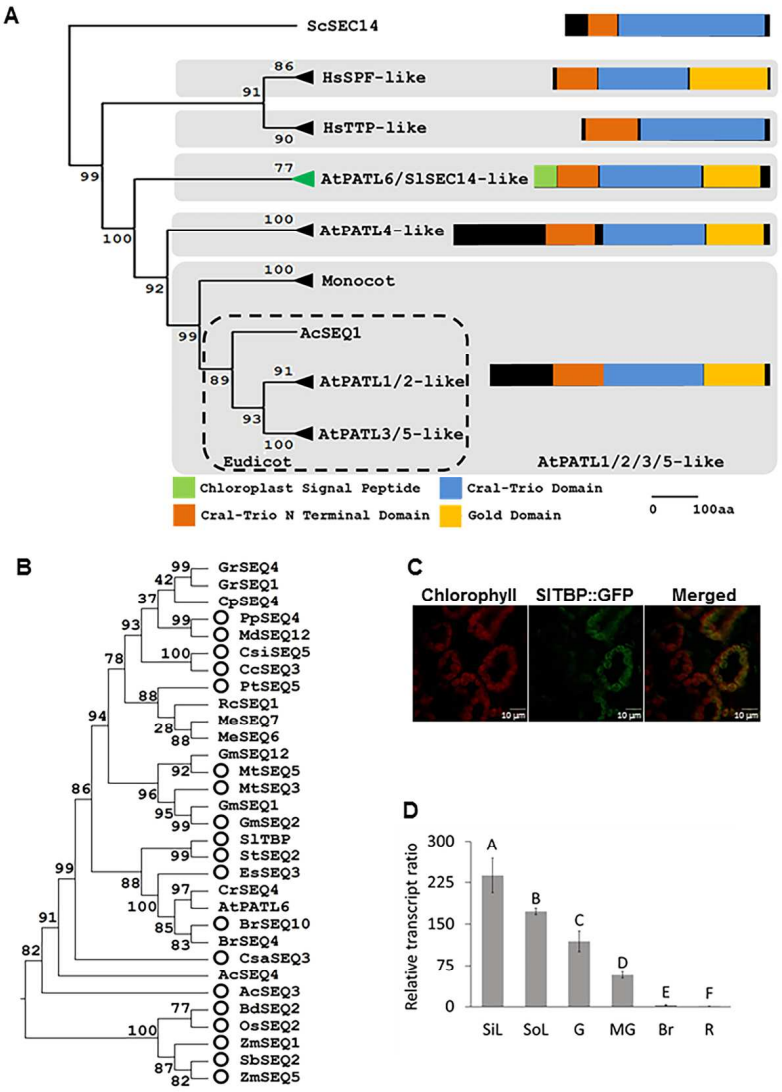

Figure 1

190x275mm (300 x 300 DPI)

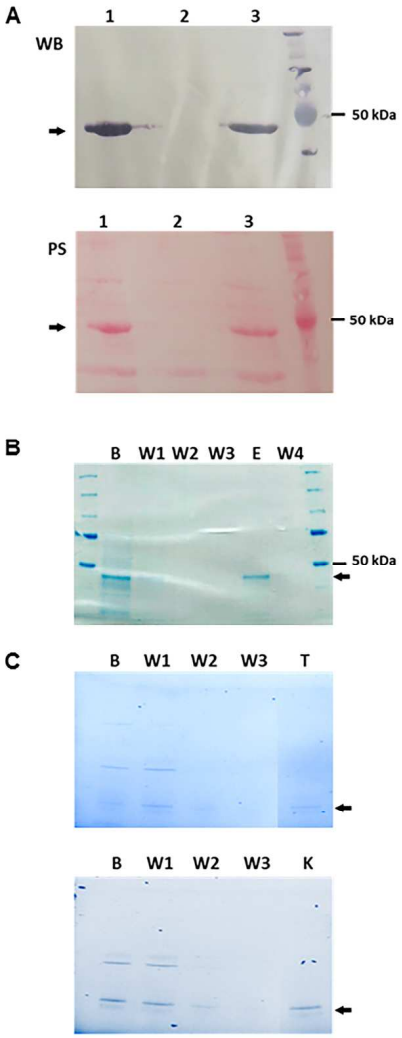

Figure 2

190x275mm (300 x 300 DPI)

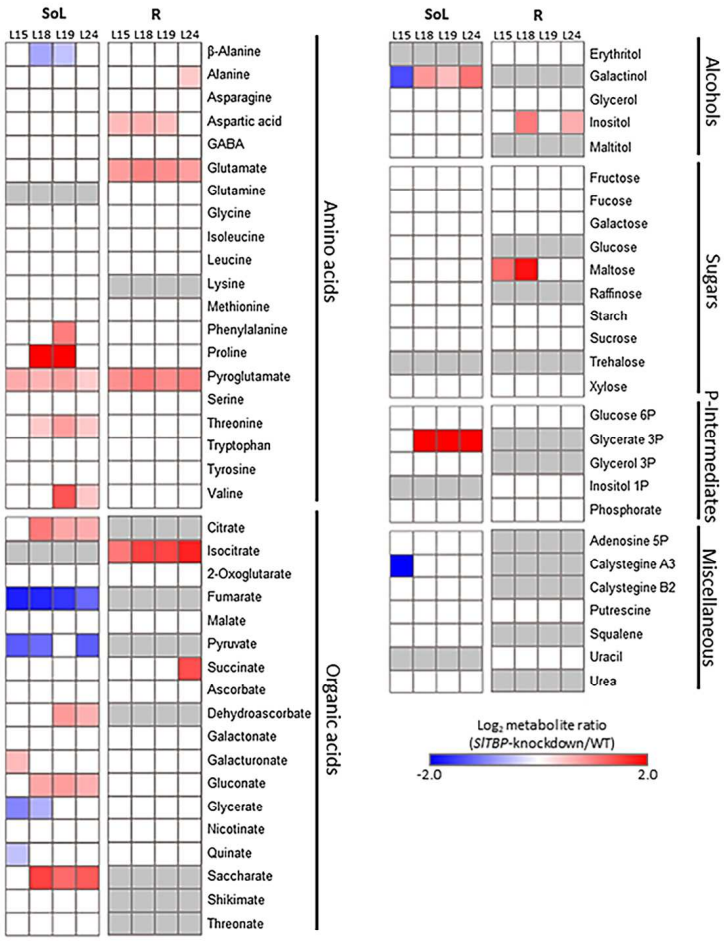

Figure 3

190x275mm (300 x 300 DPI)

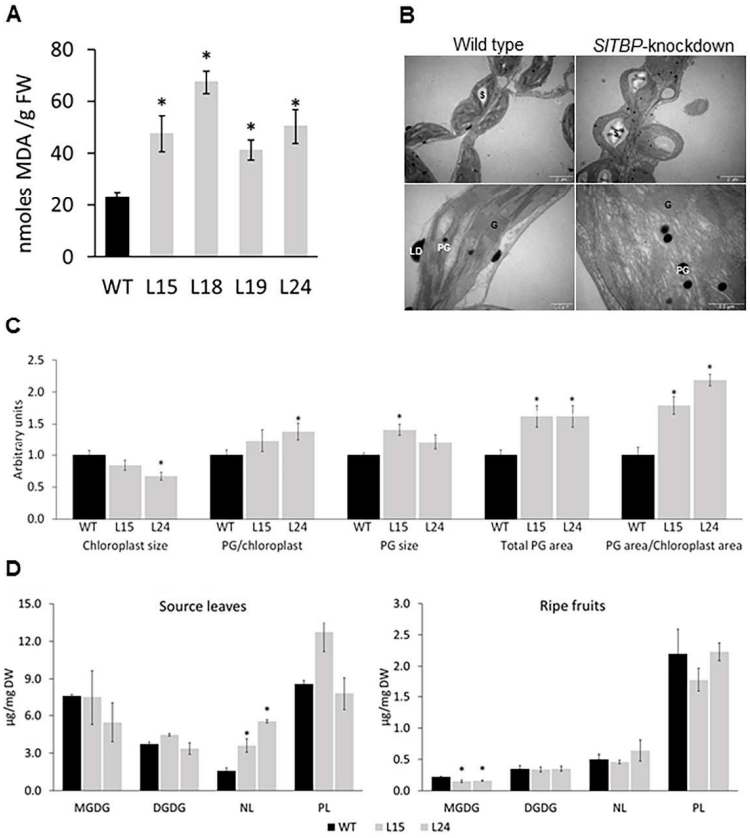

Figure 4

190x275mm (300 x 300 DPI)

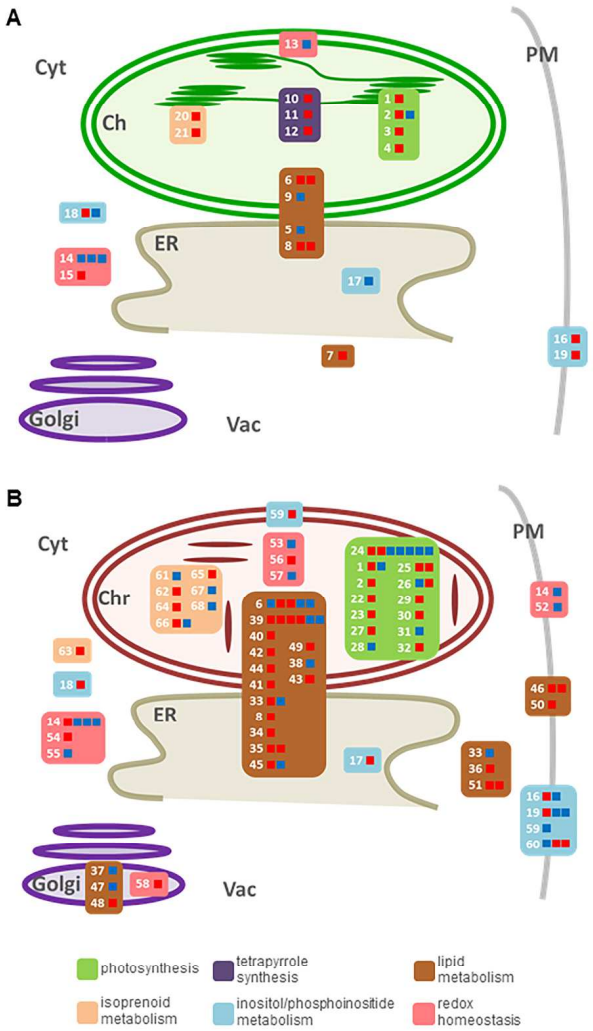

Figure 5

190x275mm (300 x 300 DPI)